2014

Relating Lagrangian and Eulerian horizontal eddy statistics in the surfzone

Spydell, Matthew S.

Spydell, M. S., F. Feddersen, R. T. Guza, and J. MacMahan (2014), Relating Lagrangian and Eulerian horizontal eddy statistics in the surfzone, J. Geophys. Res. O

AGU PUBLICATIONS

JGR

Journal of Geophysical Research: Oceans

RESEARCH ARTICLE

10.1002/2013JC009415

Key Points:
- Drifters and current meters sample the same surfzone eddies
- Surfzone Eulerian and Lagrangian statistics are related by theory
- Surfzone particle dynamics are explored

Correspondence to:
M. S. Spydell,
mspydell@ucsd.edu

Citation:
Spydell, M. S., F. Feddersen, R. T. Guza, and J. MacMahan (2014), Relating Lagrangian and Eulerian horizontal eddy statistics in the surfzone, *J. Geophys. Res. Oceans*, *119*, 1022–1037, doi:10.1002/2013JC009415.

Received 6 SEP 2013
Accepted 23 JAN 2014
Accepted article online 28 JAN 2014
Published online 12 FEB 2014

Relating Lagrangian and Eulerian horizontal eddy statistics in the surfzone

Matthew S. Spydell[1], Falk Feddersen[1], R. T. Guza[1], and Jamie MacMahan[2]

[1]Integrative Oceanography Division, Scripps Institution of Oceanography, UC San Diego, La Jolla, California, USA, [2]Oceanography Department, Naval Postgraduate School, Monterey, California, USA

Abstract Concurrent Lagrangian and Eulerian observations of rotational, low-frequency (10^{-4} to 10^{-2} Hz) surfzone eddies are compared. Surface drifters were tracked for a few hours on each of 11 days at two alongshore uniform beaches. A cross-shore array of near-bottom current meters extended from near the shoreline to seaward of the surfzone (typically 100 m wide in these moderate wave conditions). Lagrangian and Eulerian mean alongshore velocities V are similar, with a midsurfzone maximum. Cross-shore dependent Lagrangian (σ_L) and Eulerian (σ_E) rotational eddy velocities, estimated from low-pass filtered drifter and current meter velocities, respectively, also generally agree. Cross-shore rotational velocities have a midsurfzone maximum whereas alongshore rotational velocities are distributed more broadly. Daily estimates of the Lagrangian time scale, the time for drifter velocities to decorrelate, vary between 40 and 300 s, with alongshore time scales greater than cross-shore time scales. The ratio of Lagrangian to apparent Eulerian current meter decorrelation times T_L/T_A varies considerably, between about 0.5 and 3. Consistent with theory, some of the T_L/T_A variation is ascribable to alongshore advection and T_L/T_A is proportional to V/σ, which ranges between about 0.6 and 2.5. Estimates of T_L/T_A vary between days with similar V/σ suggesting that surfzone Lagrangian particle dynamics vary between days, spanning the range from "fixed-float" to "frozen-field" [*Lumpkin et al.*, 2002], although conclusions are limited by the statistical sampling errors in both T_L/T_A and V/σ.

1. Introduction

Eddy-induced tracer transport and dispersion is important at many scales in the ocean, including the surfzone. On 10^3 km horizontal scales, eddies are an important component of the meridional eddy temperature flux [e.g., *Marshall et al.*, 2006; *Ferrari and Nikurashin*, 2010; *Abernathey and Marshall*, 2013]. At the other extreme, turbulence at cm scales sets the interior ocean vertical eddy diffusivity, critical to the overturning circulation [*Wunch and Ferrari*, 2004]. The surfzone vertical eddy diffusivity is also set by cm scale turbulence [*Feddersen*, 2012b]. The horizontal surfzone eddies considered here have scales greater than the water depth ($h \leq 5$ m), and affect the cross-shore flux of pathogens [e.g., *Rippy et al.*, 2013a; *Feng et al.*, 2013], larvae [*Defeo and McLachlan*, 2005], bubbles [e.g., *Ma et al.*, 2011], and likely sediment.

Many numerical models of geophysical flows do not resolve horizontal eddies or their generation mechanism, and eddy-induced fluxes (of a tracer ϕ) often are parameterized as

$$\langle u'\phi' \rangle = -K\frac{\partial \bar{\phi}}{\partial x} \tag{1}$$

where $\langle\rangle$ denotes an ensemble average, $'$ is the fluctuating component, u is the fluid velocity in the x direction, $\bar{\phi}$ is the mean tracer, and K is the eddy diffusivity. *Taylor* [1922] showed that the eddy diffusivity can be found from Lagrangian (drifter) observations

$$K = \int_0^\infty C_L(t')dt', \tag{2}$$

where K is the long-time eddy diffusivity and

$$C_L(t) = \langle u_L'(t'+t) u_L'(t') \rangle, \tag{3}$$

is the Lagrangian velocity autocovariance, where u_L' is the Lagrangian eddy velocity (i.e., the mean flow is removed) and $\langle\rangle$ represents an ensemble average over independent drifter trajectories. Defining the Lagrangian time scale

$$T_L = \frac{1}{\sigma_L^2} \int_0^\infty C_L(t') dt', \tag{4}$$

where $\sigma_L^2 = C_L(0)$ is the Lagrangian velocity variance, yields

$$K = \sigma_L^2 T_L. \tag{5}$$

Thus, understanding what sets the Lagrangian time scale T_L is critical to parameterizing the eddy diffusivity K.

The eddy diffusivity K can be estimated either directly from Lagrangian drifters or from tracer observations. In the open ocean, vertical K has been estimated from the spreading of a tracer patch [*Ledwell et al*., 2000] and horizontal K from satellite-tracked drifters [e.g., *Lumpkin et al*., 2002; *Zhurbas and Oh*, 2004; *Rypina et al*., 2012] as well as eddy-resolving numerical model tracer output [e.g., *Abernathey and Marshall*, 2013]. Horizontal K has also been estimated using model output, dye, and drifters on the continental shelf [e.g., *Dever et al*., 1998], and in the surfzone [e.g., *Spydell et al*., 2007; *Spydell and Feddersen*, 2009; *Brown et al*., 2009; *Clark et al*., 2010].

However, as observations are often Eulerian, and turbulence (eddies) is often described from an Eulerian perspective (e.g., wave number spectra), how the eddy diffusivity K, a Lagrangian statistic, should be parameterized in terms of Eulerian statistics has attracted significant attention. For nondivergent flows with spatially unbiased sampling, Lagrangian and Eulerian eddy velocities are theoretically equal $\sigma_L = \sigma_E = \sigma$ [e.g., *Davis*, 1983]. The Lagrangian autocovariance function (3) is related to Eulerian velocity statistics and particle spreading by assuming that particle displacements are statistically independent of the velocity field (known as "Corrsin's conjecture") [*Corrsin*, 1959]. The relationship between Eulerian and Lagrangian statistics has been explored by using Corrsin's conjecture with specific turbulent-like forms of Eulerian statistics and assuming Gaussian particle spreading [*Saffman*, 1963; *Philip*, 1967; *Davis*, 1982; *Middleton*, 1985]. With no mean flow, the ratio of Lagrangian to Eulerian time scales (T_L/T_E) depend on the nondimensional parameter $\alpha = \sigma T_E / L_E$, where L_E is the Eulerian length scale, the eddy size. With a mean flow V, T_L/T_E depends also on the turbulence intensity (σ/V) [*Middleton*, 1985].

Here the relationship between surfzone Lagrangian and Eulerian eddy statistics, and the estimation of the eddy diffusivity K from Eulerian observations, is explored. In section 2, theory and conceptual models relating Lagrangian and Eulerian velocity statistics are reviewed briefly. Deployments of drifters and fixed current meters on two alongshore uniform beaches, and the analysis methodology, are described in section 3. Lagrangian and Eulerian observations are compared in section 4, discussed in section 5, and summarized in section 6.

2. Theoretical Background

One (x) dimension is considered for simplicity. Extension to two dimensions is straightforward. The Lagrangian velocity time series is $u_L(t) = dX/dt$ with $X(t)$ the drifter position. Eulerian and Lagrangian velocities are related by $u_L(t) = u_E(X(t), t)$, i.e., the Lagrangian velocity at t is the Eulerian velocity measured at $X(t)$. With no mean flow, and for homogeneous, isotropic, and stationary turbulence, $u_L'(t) = u_L(t) = u_E(X(t))$ and (3) is

$$C_L(t) = \langle u_L(t) u_L(0) \rangle = \langle u_E(X(t), t) u_E(0, 0) \rangle, \tag{6}$$

where the initial release location and time are $X = 0$ and $t = 0$. Assuming $X(t)$ are random and independent of velocity statistics,

$$C_L(t)=\langle u_E(X(t),t)u_E(0,0)\rangle=\int\langle u_E(r,t)u_E(0,0)\rangle P(r,t)dr \tag{7}$$

where $P(r,t)$ is the probability distribution function of particle displacements r. Thus, it is not necessary to have Gaussian particle displacements in order to relate Eulerian and Lagrangian statistics. Corrsin's conjecture (7) has been examined theoretically [*Saffman*, 1963; *Weinstock*, 1976] and if $P(r,t)$ is Gaussian, then displacements do *not* need to be assumed independent of the velocities [*Zhang*, 1995].

Defining the Eulerian space-lagged and time-lagged autocovariance function $C_E(r,t)=\langle u_E(r,t)u_E(0,0)\rangle$,

$$C_L(t)=\int C_E(r,t)P(r,t)dr. \tag{8}$$

Equation (8) is transformed into a nonlinear ODE for particle displacement variance $D(t)$ using $2C_L(t)=d^2D(t)/dt^2$ [*Taylor*, 1922] and $P(r,t)=P(r,D(t))$,

$$\frac{d^2D}{dt^2}=2\int C_E(r,t)P(r,D)dr. \tag{9}$$

For a variety of Eulerian statistics $C_E(r,t)$, Lagrangian statistics (i.e., D) have been determined from (9) using initial conditions $D(0)=dD(0)/dt=0$ and Gaussian displacements $P(r)$ [e.g., *Philip*, 1967; *Lundgren and Pointin*, 1976; *Middleton*, 1985]. The central result of these studies is that for no mean flow, the Lagrangian to Eulerian time scale ratio T_L/T_E only depends on a single nondimensional parameter α

$$T_L/T_E=f(\alpha)\quad\text{where}\quad\alpha=\sigma T_E/L_E. \tag{10}$$

The Eulerian parameter α is the ratio of the Eulerian decorrelation time scale T_E, which for a nonzero mean flow needs to be measured in a reference frame that moves with the mean flow, to the eddy crossing time L_E/σ, where L_E is the eddy length scale. The eddy crossing time assumes that the eddy field is effectively "frozen" so that the field does not evolve in time before a particle crosses an eddy. Both T_E and L_E are integral properties of C_E, with T_E defined similarly to T_L in (4) and, appropriate for spatially periodic turbulence, L_E is typically defined from the wave number spectra $L_E=2\sigma^{-2}\int_0^\infty k^{-1}S(k)dk$ where $S(k)$ is the velocity wave number spectra. As *Philip* [1967] anticipated, and *Middleton* [1985] demonstrated, T_L/T_E is determined by the bulk properties of $C_E(r,t)$ (i.e., σ, T_E, and L_E), rather than $C_E(r,t)$'s specific form. In general, T_L/T_E is a decreasing function of $\alpha=\sigma T_E/L_E$ [*Philip*, 1967; *Middleton*, 1985] and (for no mean flow) $T_L/T_E\leq 1$ always.

Middleton [1985] found that for the T_E and L_E definitions above, and assuming Gaussian displacements,

$$T_L/T_E=\frac{q}{\sqrt{q^2+\alpha^2}} \tag{11}$$

where $q=(\pi/8)^{1/2}$. As (11) is within 10% for various forms of $C_E(r,t)$ [*Middleton*, 1985], (11) is also valid for non-Gaussian displacements and the general inverse dependence of T_L/T_E on α does not depend on $P(r,t)$'s specific form. Using (11), the eddy diffusivity (5) is

$$K=\sigma^2\frac{q}{\sqrt{q^2+\alpha^2}}T_E \tag{12}$$

and K depends only on Eulerian statistics. For small and large α, solving for T_L in (11)

$$T_L\approx\begin{cases}T_E & \text{for } \alpha\ll 1\\ qL_E/\sigma & \text{for } \alpha\gg 1\end{cases} \tag{13}$$

leads to the eddy diffusivity parameterizations

$$K \approx \begin{cases} \sigma^2 T_E & \text{for } \alpha \ll 1 \\ q\sigma L_E & \text{for } \alpha \gg 1. \end{cases} \quad (14)$$

In the "fixed-float" regime $\alpha \ll 1$, the eddy crossing time for a drifter (L_E/σ) is much greater than the eddy life time (T_E) so a drifter samples only part of an eddy before the eddy evolves. Thus, drifter and current meter velocity time series are similar such that $T_L \approx T_E$ and $K \approx \sigma^2 T_E$. In the "frozen-field" regime $\alpha \gg 1$, the Lagrangian decorrelation time is determined by the eddy crossing time $T_L \approx qL_E/\sigma$ and a classic mixing-length scaling $K \approx q\sigma L_E$ applies for the eddy diffusivity. Conceptually, in frozen-field turbulence a drifter wanders across many disparate eddies before the eddy field evolves resulting in $T_L < T_E$.

These theoretical relationships for T_L/T_E have been explored in atmospheric boundary layer [*Anfossi et al*., 2006] and oceanic settings (such as the N. Atlantic [*Lumpkin et al*., 2002], the Northern California Shelf [*Davis*, 1985], and the Tasman sea and Southern Ocean [*Chiswell et al*., 2007]) that are not homogeneous or isotropic, and also have boundaries. Using the critical α values as defined in *Lumpkin et al*. [2002], the open ocean eddy field ranges from fixed-float ($\alpha < 0.5$) to frozen-field ($\alpha > 1$) [*Lumpkin et al*., 2002; *Chiswell et al*., 2007]. Surfzone α is discussed in section 5.1.

When a mean velocity V advects eddies past a fixed current meter, the apparent decorrelation time T_A of current meter velocities is less than the eddy time scale T_E measured with $V = 0$. How much less depends on the turbulent intensity $I = \sigma/V$ [*Philip*, 1967; *Middleton*, 1985]. Middleton showed that (within 30%)

$$T_L/T_A \approx \frac{q(1+3\alpha^2 I^{-2})^{1/2}}{(q^2+\alpha^2)^{1/2}}. \quad (15)$$

For weak $V(I \gg 1)$, (15) reverts to (11). For strong $V(I \ll 1), T_L/T_A \sim V/\sigma$, as in the atmospheric boundary layer [*Anfossi et al*., 2006] and wind tunnels [*Koeltzsch*, 1998].

The surfzone, similar to the atmospheric boundary layer, is neither homogeneous nor isotropic. For such conditions, a complete theoretical description relating Eulerian and Lagrangian statistics does not exist. To account for anisotropy, following *Anfossi et al*. [2006], directions are assumed independent and I is broken down into components: $I_u = \sigma_u/V$ and $I_v = \sigma_v/V$.

3. Data and Methods

3.1. Data Overview

Lagrangian surfzone data were collected on 5 days during the Fall 2006 Huntington Beach experiment (HB06) [*Spydell et al*., 2009; *Clark et al*., 2010; *Omand et al*., 2011; *Feddersen*, 2012b; *Rippy et al*., 2013a] and 6 days at the Fall 2009 Imperial Beach experiment (IB09) [*Feddersen*, 2012a; *Rippy et al*., 2013b] using GPS-equipped drifters sampling at 1 Hz [*Schmidt et al*., 2003; *MacMahan et al*., 2009]. Drifter results from IB09 have not been described previously. For all 5 HB06 days, and on 3 of the 6 IB09 days, 10 drifters were deployed simultaneously resulting in about 20 drifter h/d. For the 3 other IB09 days, 35 drifters were deployed simultaneously resulting in about 80 drifter h/d. At HB06 and IB09, most drifters sampled the surf-zone, hence the Lagrangian statistics presented here represent surfzone mixing and do not represent the longer time scale dispersion governed by inner-shelf dynamics. Drifters were released for 4–6 h of each day and individual drifter trajectories averaged approximately 1000 s with a few trajectories over 2000 s [e.g., *Spydell et al*., 2009]. Days are denoted by HB06d1 for HB06 day 1, HB06d2 for HB06 day 2, etc. At both sites (x, y), are the cross-shore and alongshore coordinates with x increasing onshore and $x = 0$ m at the mean shoreline. Although dependent on wave conditions that varied daily, at both HB06 and IB09 the typical surf-zone width was approximately 100 m [*Spydell et al*., 2009; *Clark et al*., 2010]. HB06 and IB09 bathymetry are both alongshore uniform (see Figures 1a and 1b) with IB09 bathymetry steeper near the shoreline. At HB06 (Figure 1a), all drifter data were utilized. At IB09 (Figure 1b) only drifter tracks within $-550 < y < 75$ m are considered. Drifters are deemed too far from the current meters when $y < -550$ m, and drifters are too close to a pier ($y = 250$ m) when $y > 75$ m. A cross-shore array of seven and six ADV current meters (Figure 1 green x's) sampling at 8 Hz were deployed at HB06 and IB09, respectively, in mean depths between 1 and 4 m at $y = 0$ m.

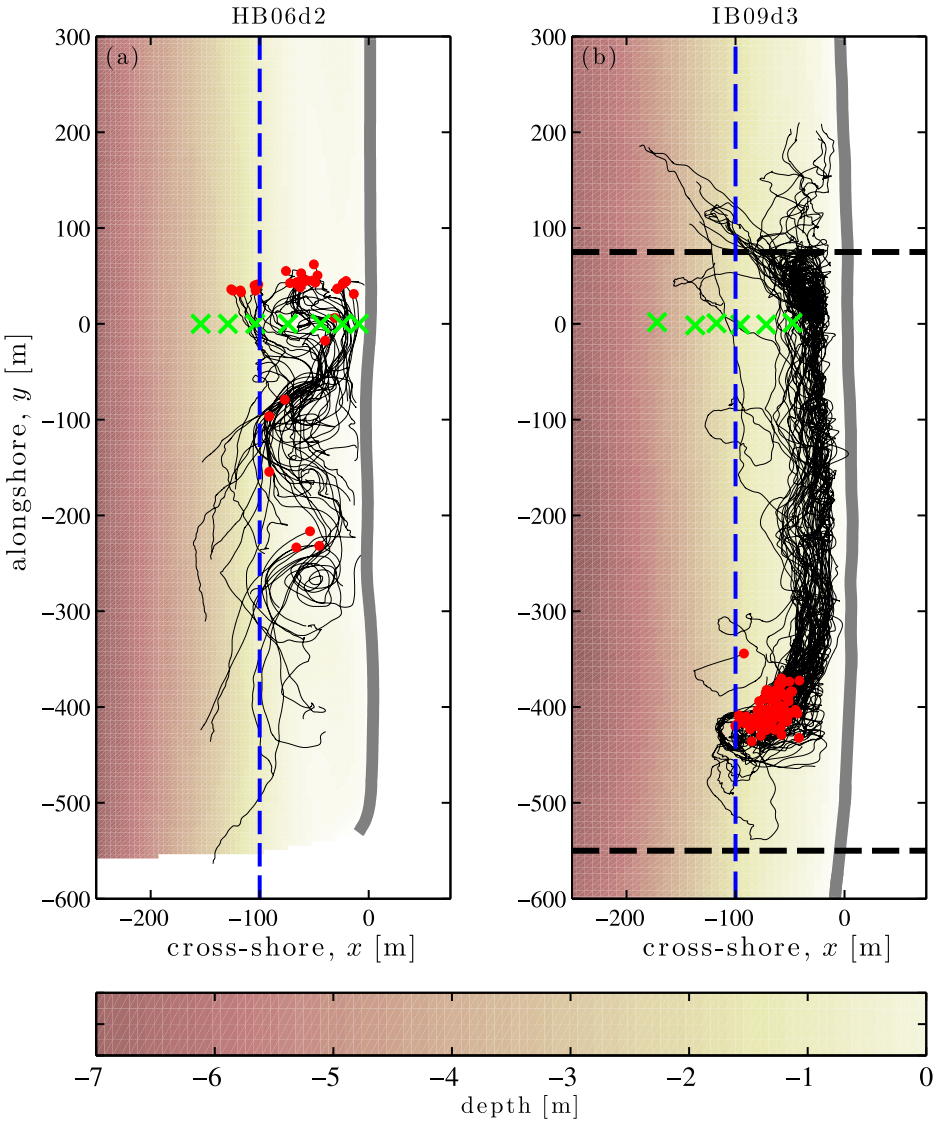

Figure 1. Drifter tracks at (a) HB06 on day 2 and (b) IB09 on day 3. Red dots indicate drifter release locations and green x's denote current meter locations. Bathymetry is colored and the thick gray line is the shoreline. Vertical dashed blue lines indicate surfzone widths and horizontal dashed lines in Figure 1b indicate the region where Lagrangian data are analyzed.

3.2. Estimating Lagrangian Statistics

Lagrangian velocity statistics are assumed temporally stationary, alongshore homogeneous, and cross-shore variable. Although not strictly alongshore homogeneous, variation in Lagrangian velocity statistics is strongest in the cross-shore direction (addressed in section 4.1.1). Lagrangian horizontal velocities $(\tilde{u}_L(t), \tilde{v}_L(t))$ were calculated by finite differencing positions $(X(t), Y(t))$. Low-frequency velocities $(u_L(t), v_L(t))$, from which Lagrangian time scales are estimated, are isolated by filtering velocities with a low-pass Gaussian filter with a time scale of $\tau_F = 30$ s. If the true time scale were less than $\tau_F = 30$ s, then the inferred T_L would be improperly set to 30 s. However, the minimum inferred $T_L = 40$ s, indicating that the filtering is not affecting the T_L estimates.

The filtered velocities contain both rotational and irrotational (gravity wave) motions. Rotational (eddy) velocities are the ones that drive drifter dispersion [*Spydell and Feddersen*, 2009] and are generally stronger than irrotational motions at $f < 0.01$ Hz [e.g., *MacMahan et al.*, 2010]. In the infragravity frequency band $(0.01 < f < 0.03\,\text{Hz})$, both rotational and irrotational motions can be present [e.g., *Noyes et al.*, 2004; *Feddersen et al.*, 2011]. Thus, in order to minimize the irrotational contribution to the low-frequency Lagrangian

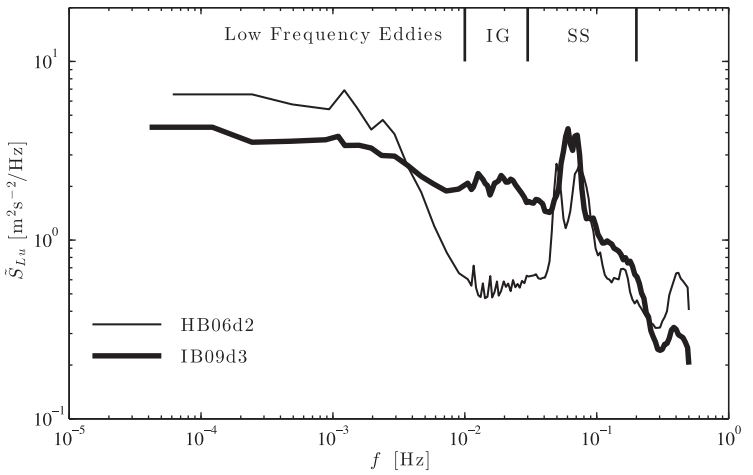

Figure 2. The spectra $(\bar{S}_{Lu})$ of unfiltered 1 Hz Lagrangian (drifter) cross-shore velocities versus frequency for HB06d2 (thin black line) and IB09d3 (thick black line). The low frequency eddies (LFE), infragravity (IG), and sea-swell (SS) frequency bands are indicated. IB09d3 lacks a spectral valley separating LFE from IG/SS bands.

velocity variance, the analysis is limited to cases when the unfiltered daily Lagrangian velocity spectra had a clear scale separation (defined as a spectral valley) within the IG frequency band. The presence of a velocity scale separation was determined by visual inspection of the unfiltered daily Lagrangian velocity power spectra. For example, cross-shore velocity spectra on HB06d2 had a distinct scale separation, whereas IB09d3 spectra did not (thin and thick curves in Figure 2, respectively). Cross-shore velocity spectra had scale separation on all 5 HB06 days and 1 IB09 (IB09d6) day. Alongshore velocity spectra had scale separation on all HB06 and IB09 days. Although HB06d2 tracks (Figure 1a) showed the strongest eddy activity of any day considered, eddy activity is not necessary for a cross-shore velocity spectra scale separation as all other HB06 days had a cross-shore velocity scale separation and had drifter tracks which showed much less eddy activity. The HB06d4 alongshore data set was discarded as HB06d4 drifters converged at the shoreline resulting in anomalous Lagrangian alongshore statistics [e.g., *Spydell et al*., 2009]. Thus, this results in 6 cross-shore and 10 alongshore data sets to analyze.

The rotational velocities $(u_L(t), v_L(t))$ were sorted by cross-shore position $X(t)$ in seven bins with edges at the ADV cross-shore locations. ADV position bin edges are chosen so that Eulerian and Lagrangian statistics are readily compared when plotting, however, bin centers are usually not at ADV midpoints because drifter distributions are nonuniform within bins. Time averaging yields cross-shore dependent mean velocities, $U_L(x)$ and $V_L(x)$. The fluctuating Lagrangian alongshore velocity is

$$v'_L(t) = v_L(t) - V_L(X(t)) \tag{16}$$

where the observed cross-shore dependent mean velocity $V_L(x)$ is linearly interpolated to X. The alongshore eddy velocity $s_{Lv}(x)$ is the standard deviation of $v'_L(x,t)$

$$s^2_{Lv}(x) = \langle v'^2_L(x,t) \rangle \tag{17}$$

where $\langle\rangle$ is an average over all v' in a bin. Fluctuating cross-shore velocities are defined similarly. The cross-shore-dependent mean $V(x)$ is removed, so v'_L does not include contributions from the sheared $V(x)$. The present s are similar to s from the Lagrangian stochastic model of *Spydell and Feddersen* [2012], but differ from *Spydell et al*. [2009] where the daily bulk mean was used in (16) and the alongshore current shear was included in s. (The appropriateness of including shear in v' depends on the application.)

The daily bulk Lagrangian alongshore velocity is

$$\bar{V}_L = \langle v_L(t) \rangle, \tag{18}$$

where the average $\langle\rangle$ is over all trajectories and times in a day. Daily bulk quantities are effectively averages of cross-shore dependent variables (of $V_L(x)$ for example) weighted by the proportional time drifters spent at different cross-shore locations. The 4–6 h overall duration of daily drifter releases gives the effective time averaging used to determine Lagrangian statistics such as $\bar{V}_L$. The daily bulk Lagrangian velocity

autocovariance function $C_L(t)$ is calculated using v' in (3) and the average $\langle\rangle$ in (3) is over all trajectories and all time lags t' on each trajectory (see Figures 3a and 3b for representative HB06d2 cross-shore and alongshore $C_L(t)$).

3.2.1. Fitting

Lagrangian cross-shore and alongshore rotational velocity variances, σ^2_{Lu} and σ^2_{Lv}, and Lagrangian time scales, T_{Lu} and T_{Lv}, are found by least-squares fitting an exponential to the daily bulk cross-shore and alongshore velocity autocovariance function $C_L(t)$ [similar to *Pope*, 1994; *Garraffo et al*., 2001; *Sallée et al*., 2008; *Chiswell and Rickard*, 2008; *Spydell et al*., 2009]. Specifically, σ^2_L, and T_L are found by minimizing

$$\min_{\sigma^2_L, T_L} \int_{20\,\mathrm{s}}^{600\,\mathrm{s}} [C_L(t) - \sigma^2_L \exp(-t/T_L)]^2 dt. \tag{19}$$

The fitting of $C_L(t)$ is restricted to $20 \le t \le 600$ s. Although $C_L(t)$ only depends weakly on the choice of the low-pass velocity filter's cutoff frequency f_c for $t < 20$ s, due to the insistence of a frequency-scale separation between eddies and IG motions, this effect is removed by choosing a lower limit of $t = 20$ s for the fitting. The upper limit $t = 600$ s is chosen because for $t < 600$s, the $C_L(t)$ error bars are still relatively small [for details see *Spydell and Feddersen*, 2009] and at $t = 600$ s $C_L(t)$ has decayed substantially (Figures 3a and 3b). Although the negative lobes of both cross-shore and alongshore $C_L(t)$ that sometimes occur for $t > 100$ s (Figures 3a and 3b; *Spydell and Feddersen* [2009, Figure 3]) are not fit with the exponential, these lobes are not much larger than the sampling errors in $C_L(t)$. Furthermore, T_L was not significantly altered by fitting to a functional form with a negative lobe, $\sigma^2_L \exp(-t/\tau)\cos(\omega t)$ where $T_L = \tau/(1+\omega^2\tau^2)$ [e.g., *Garraffo et al*., 2001], and both cross-shore and alongshore observed $C_L(t)$ is well fit on everyday by a simple exponential (Figure 3).

Both s_L and σ_L are measures of the rotational (eddy) velocity estimated from low-pass drifter velocities. In section 4.1.2, the similar cross-shore structure of $s_L(x)$ (17) and $s_E(x)$ (from the current meter in each bin) is shown for one day. Daily bulk Lagrangian parameters (σ_L and T_L) are estimated by fitting to daily $C_L(t)$ (19). In sections 4.1.3 and 4.2, for all days, σ_L and T_L are compared with daily bulk Eulerian values, estimated as described below.

3.3. Estimating Eulerian Statistics

The time series of unfiltered velocity of the ith current meter during hour j is $\tilde{u}_{E,ij}(t)$, and $\tilde{v}_{E,ij}(t)$ is defined similarly. On all days, $\tilde{u}_{E,ij}(t)$, and $\tilde{v}_{E,ij}(t)$, frequency spectra have a valley around 0.01 Hz, thus similar to the Lagrangian velocities, low-frequency Eulerian rotational velocities ($u_{E,ij}$) are low-passed filtered $\tilde{u}_{E,ij}$. Subtracting the time mean for each instrument and hour $U_{E,ij} = \langle u_{E,ij}(t) \rangle$, yields the fluctuating velocities $u'_{E,ij}(t) = u_{E,ij}(t) - U_{E,ij}$. The standard deviation of $u'_{E,ij}(t)$ is $s_{Eu,ij}$, the Eulerian rotational eddy velocity for the ith current meter during hour j. Thus, $s_{Eu,ij}$ is the hourly eddy velocity at each current meter. Low-pass filtered Eulerian velocities are representative of the rotational velocity field. The bulk rotational velocity $\mathcal{V}_{\mathrm{rot}}$ [e.g., *Clark et al*., 2010], estimated from colocated pressure

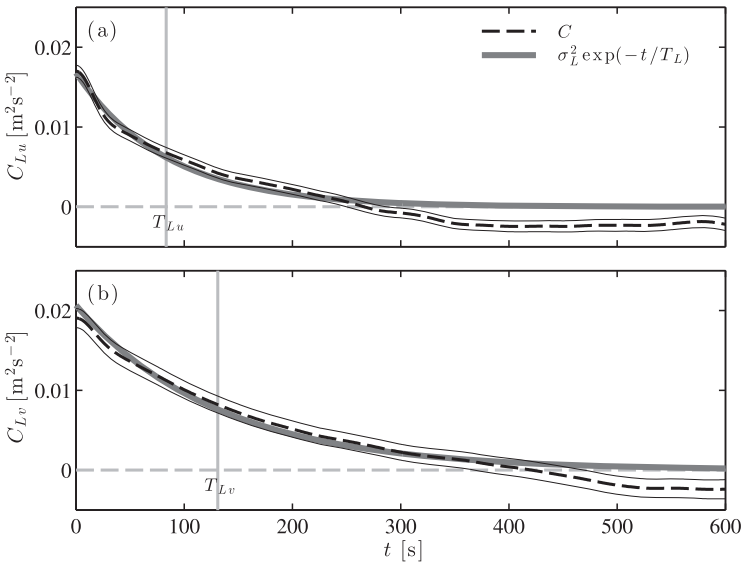

Figure 3. Lagrangian autocovariance functions C_L versus time t for HB06d2: (a) cross-shore and (b) alongshore velocity. Dashed black lines are observed $C_L(t)$ and the thick gray curve is the best fit function $\sigma^2_L \exp(-t/T_L)$. Sampling error, $\pm\epsilon_{C_L}$ are indicated about $C_L(t)$ as thin solid lines. The best fit cross-shore and alongshore Lagrangian time scales T_{Lu} and T_{Lv} are indicated.

sensors and current meters for $f < 0.03$ Hz [*Lippmann et al.*, 1999], and the low-frequency eddy velocity magnitude $|s| = (s_{Eu,ij}^2 + s_{Ev,ij}^2)^{1/2}$ (also for $f < 0.03$ Hz) are correlated ($R^2 = 0.9$) with slope 0.8 for HB06 instrument hourly values during drifter releases.

For comparison with daily bulk Lagrangian velocity statistics, current meter data are weighted by the drifter position-time weight

$$w_{ij} = N_{ij} / \sum_i \sum_j N_{ij} \tag{20}$$

where N_{ij} is the number of drifter observations in the cross-shore bin near current meter i during hour j. The daily cross-shore drifter distribution is $\mathcal{W}(x_i) = \sum_j w_{ij}$. The daily bulk mean Eulerian alongshore current is a cross-shore weighted, time average

$$\bar{V}_E = \sum_i \sum_j w_{ij} V_{E,ij}. \tag{21}$$

The cross-shore dependent mean (averaged over time, j) Eulerian alongshore velocity $V_E(x_i)$ is

$$V_E(x_i) = \sum_j W_{ij} V_{E,ij}$$

where $W_{ij} = w_{ij} / \sum_k w_{ik}$. Cross-shore dependent eddy velocities (e.g., $s_{Eu}(x)$) are defined similarly

$$s_{Eu}(x_i) = \left[\sum_j W_{ij} (s_{Eu,ij})^2 \right]^{1/2}.$$

Eulerian autocovariances for each instrument (i) and hour (j) are denoted by $C_{E,ij}$ and found using Eulerian velocities $u'_{E,ij}(t)$ in (3). The daily bulk Eulerian autocovariance is

$$C_E(t) = \sum_i \sum_j w_{ij} C_{E,ij}(t).$$

The Eulerian bulk velocity variances $(\sigma_{Eu}^2, \sigma_{Ev}^2)$ and apparent time scales (T_{Au}, T_{Av}) are found using the same fitting procedure used to determine the Lagrangian counterparts (section 3.2.1) and represent daily (time and cross-shore averaged) quantities.

4. Results: Relating Eulerian and Lagrangian Statistics

4.1. Mean Currents and Rotational Eddy Velocities

First, for one representative day (HB06d1), the cross-shore and temporal variability of Eulerian eddy velocities are examined. Cross-shore dependence of Lagrangian and Eulerian mean currents, and rotational eddy velocities are then compared for that day. Daily bulk Eulerian and Lagrangian statistics (time and cross-shore averaged) for all days are then examined.

4.1.1. Eulerian Eddy Velocities on 1 Day

Eddy velocities depend on both cross-shore position and time. Alongshore eddy velocities for the ith ADV during hour j are denoted $s_{Ev,ij}$ (see section 3.3) and indicate (HB06d1 $s_{Ev,ij}$ is shown in Figure 4) that eddy velocities vary more in the cross-shore than in time. During the 6 h of drifter releases on this day, the alongshore hourly eddy velocity changes by about 0.05 m s^{-1} for a given ADV. In contrast, at a given time, the hourly eddy velocity difference across the surfzone (i.e., between ADV1 and ADV7) is about 0.1 m s^{-1}. Thus, although the assumption of stationary statistics is not strictly met, the data are more stationary than cross-shore homogeneous.

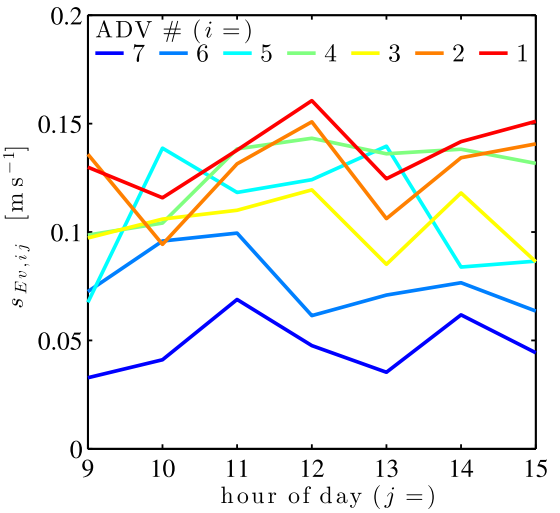

Figure 4. HB06d1 Eulerian alongshore eddy velocities ($s_{Ev,ij}$) at each ADV (i) versus time of day (j). ADV7 is farthest offshore ($h \approx 4$ m) and ADV1 closest to the shoreline ($h \approx 1$ m, see Figure 1).

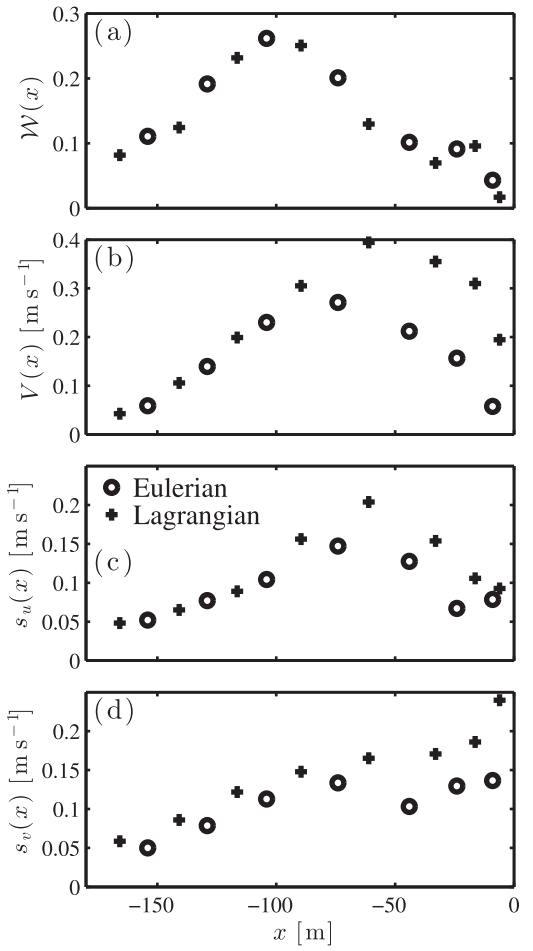

Figure 5. Observed Lagrangian (+'s) and Eulerian (o's) statistics versus cross-shore distance for HB06d1: (a) drifter cross-shore distribution $\mathcal{W}(x)$, (b) the mean alongshore velocity $V(x)$, (c) the cross-shore eddy velocity $s_u(x)$, and (d) the alongshore eddy velocity $s_v(x)$. Note that the y scale in Figure 5b is almost two times that in Figures 5c and 5d.

4.1.2. Cross-Shore Dependence on 1 Day

Averaging hourly statistics (V_{ij} and $s_{E,ij}$) over the time of drifter releases (see section 3.3) indicates that cross-shore dependent Lagrangian and Eulerian $V(x)$, $s_u(x)$, and $s_v(x)$ compare well (Figures 5b–5d), similar to HB06 cases discussed in *Spydell and Feddersen* [2009] and *Spydell and Feddersen* [2012]. The Lagrangian and Eulerian mean alongshore current $V(x)$ has a midsurfzone maximum (≈ 0.3 m s^{-1}, Figure 5b), as does the cross-shore eddy velocity $s_u(x)$ (≈ 0.2 m s^{-1}, Figure 5c). Lagrangian mean alongshore currents are larger than Eulerian near the shoreline ($x > -75$ m) on this day, however, this corresponds to an area of minimal drifter sampling (Figure 5a). Lagrangian and Eulerian alongshore eddy velocities $s_v(x)$, the standard deviation of low-frequency velocities, both have broad cross-shore distributions with weak shoreline maximum (≈ 0.15 m s^{-1}, Figure 5d). The cross-shore structure of cross-shore and alongshore daily $s_E(x)$ and $s_L(x)$ are similar [e.g., *Spydell and Feddersen*, 2012], but Lagrangian $s_u(x)$ and $s_v(x)$ are about 20–30% larger than their Eulerian counterparts within the surfzone ($x < -100$m). Although Eulerian and Lagrangian eddy velocity cross-shore dependence is similar on all days, the magnitude of this Lagrangian/Eulerian difference depends on the day. The similarity of basic Lagrangian and Eulerian statistics (Figures 5b–5d) supports the basic assumption that vertical variations are weak and drifters and current meters sample the same surfzone low-frequency eddy field. Because surfzone eddies have length scales (>10 m, see tracks in Figure 1a) larger than the depth (<5 m), vertical variation is not

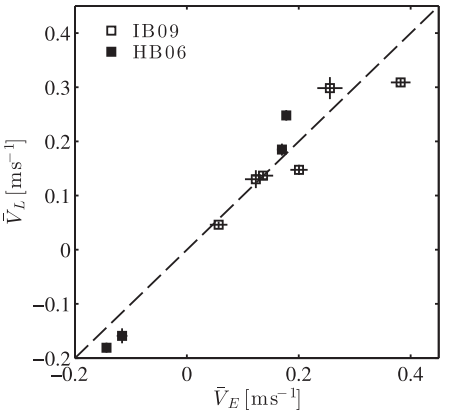

Figure 6. Daily bulk Lagrangian $\bar{V}_L$ versus daily bulk Eulerian $\bar{V}_E$ mean alongshore velocity from both HB06 (circles) and IB09 (squares). Sampling errors are indicated as crosshairs and the one-to-one line is dashed.

expected as shallow water dynamics should apply. Thus, it is assumed that larger Lagrangian than Eulerian surfzone eddy velocities (Figures 5c and 5d) are not due to drifters and current meters sampling different vertical parts of the flow.

On the other hand, mean cross-shore shore velocities depend on depth and current meters were often located within 1 m of the seafloor, in the lower half of the water column, and when in the surfzone measured an offshore Eulerian undertow U_E (0.1–0.2 m s^{-1}). Drifters, designed to duck under bores to avoid surfing ashore and grounding on the beach [*Schmidt et al.*, 2003], measured mean surface U directed both shoreward and seaward, with magnitude smaller than the current meter U_E. Hence, due to drifters and current meters sampling different vertical parts of the flow, drifter $U_L(x)$ and Eulerian $U_E(x)$ are not comparable.

4.1.3. Daily Bulk Estimates

Daily bulk Lagrangian alongshore velocity $\bar{V}_L$ are estimated by averaging all alongshore velocity drifter observations (18), and for comparison daily bulk Eulerian $\bar{V}_E$ are appropriately weighted (section 3.3). Daily bulk mean Lagrangian $(\bar{V}_L)$ and Eulerian $(\bar{V}_E)$ mean velocities compare well with velocities between -0.2 and 0.3 m s^{-1} with small RMS difference (0.03 m s^{-1}, Figure 6). Current meter cross-shore eddy velocity σ_{Eu} varies between about 0.08 and 0.11 m s^{-1} (Figure 7a), similar to eddy velocities reported for other days during HB06 [*Feddersen et al.*, 2011] and at Duck [*Noyes et al.*, 2004, 2005; *MacMahan et al.*, 2010]. Lagrangian and Eulerian alongshore eddy velocities σ_v are correlated (Figure 7b), and $\sigma_{Lv} \approx 1.4\sigma_{Ev}$. Similarly, in the cross-shore, $\sigma_{Lu} > \sigma_{Eu}$, although the correlation is not significant. Although for a given day, $s_{Lu}(x)$ and $s_{Eu}(x)$ are correlated (Figure 5c) when weighted (by drifter cross-shore position), daily bulk values of σ_{Lu} and σ_{Eu} are not related. This suggests that the ratio between $s_{Lu}(x)$ and $s_{Eu}(x)$ differs between days or that weighting by drifter cross-shore position introduces error. Departures from unity in σ_L/σ_E ratios may result from spatial inhomogeneity in the flow field, imperfect instruments, and other factors. For instance, Lagrangian eddy velocities can be larger than Eulerian if the eddies are wave-like [*Davis*, 1982]. Differences in Lagrangian and Eulerian eddy velocity could be due to noisy data. For the data here, GPS noise in drifter position occurs when drifters are submerged under passing bores and GPS satellite lock is lost. However, as this noise is higher frequency than the eddies, only a small amount of the Lagrangian and Eulerian σ_u difference can be attributed to this source. Departures from unity in σ_L/σ_E ratios have been reported in the open ocean [e.g., *Chiswell and Rickard*, 2008].

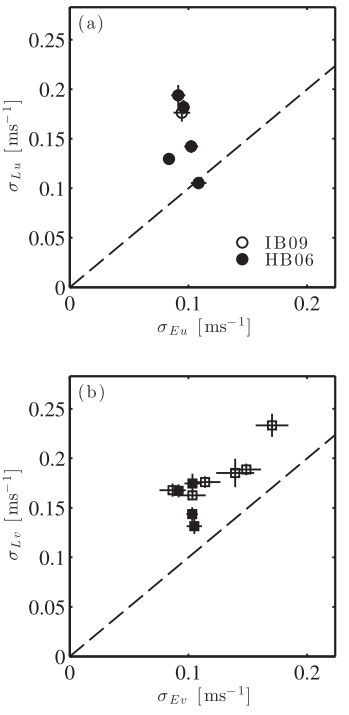

Figure 7. Lagrangian (σ_L) versus Eulerian eddy velocity (σ_E): (a) cross-shore eddy velocity, circles and (b) alongshore eddy velocity, squares. Sampling errors are indicated as crosshairs and one-to-one lines are dashed. Filled and unfilled markers represent HB06 and IB09 data, respectively.

4.2. Time Scales

Lagrangian and apparent Eulerian cross-shore time scales (T_{Lu} and T_{Au}) vary between 50 and 150 s (Figure 8a), whereas the alongshore time scales (T_{Lv} and T_{Av}) are longer, generally between 100 and 500 s (Figure 8b). Alongshore time scales are longer than cross-shore potentially due to longer

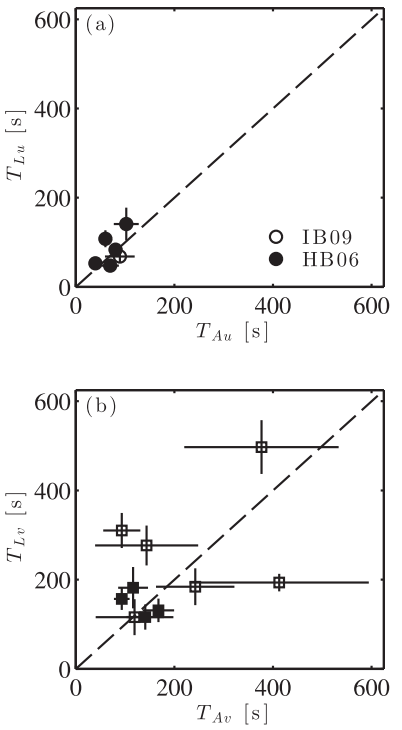

Figure 8. Lagrangian (T_L) versus apparent Eulerian time scales (T_A): (a) cross-shore, circles and (b) alongshore, squares. Sampling errors are indicated as crosshairs and one-to-one lines are dashed. Filled and unfilled markers represent HB06 and IB09 data, respectively.

alongshore eddy length scales: cross-shore eddy length scales are limited by the surfzone width whereas for alongshore uniform beaches, alongshore eddy length scales are not similarly limited. Unfortunately, definitively answering this by calculating both cross-shore and alongshore Eulerian length scale estimates is not possible without an alongshore array of current meters. Lagrangian and apparent Eulerian time scales T_L and T_A are only weakly correlated. The ratio of Lagrangian drifter to apparent Eulerian current meter decorrelation times T_L/T_A varies considerably, between about 0.5 and 3.0 (Figure 9), and some of the variation is ascribable to the relatively large range of $\bar{V}/\sigma$ (between about 0.6 and 2.5) of these observations. As $\bar{U}_L \ll \bar{V}_L$, T_{Lu}/T_{Au} depends on $I_u^{-1} = \bar{V}_E/\sigma_{Eu}$ and alongshore T_{Lv}/T_{Av} depends on $I_v^{-1} = \bar{V}_E/\sigma_{Ev}$, i.e., equation (15) [*Middleton*, 1985]. For the I^{-1} definitions, $\bar{V}_E$ was chosen instead of $\bar{V}_L$ for consistency with σ_E. For large V/σ, the time for an eddy to advect past a current meter T_A is less than the time a drifter spends in an eddy T_L, and $T_L/T_A > 1$. Alongshore advection effects are detectable in the present T_L/T_A observations (Figure 9), but estimates of T_L/T_A vary between days with similar $\bar{V}/\sigma$. Thus, T_L and T_A are related, and a single curve could be fit to the data in Figure 9 albeit with scatter. One explanation for such scatter is that the surfzone eddy field varies between days, spanning the range from "fixed-float" to "frozen-field" [*Lumpkin et al.*, 2002]; however, conclusions are limited by the substantial statistical sampling errors in both T_L/T_A and $\bar{V}/\sigma$ (crosshairs in Figure 9). Reducing the errors in these estimates, and thus discerning differences between the observations and theory, would require longer (>6 h) Eulerian velocity time series as the relative paucity of Eulerian data is the major source of error in Figures 8 and 9.

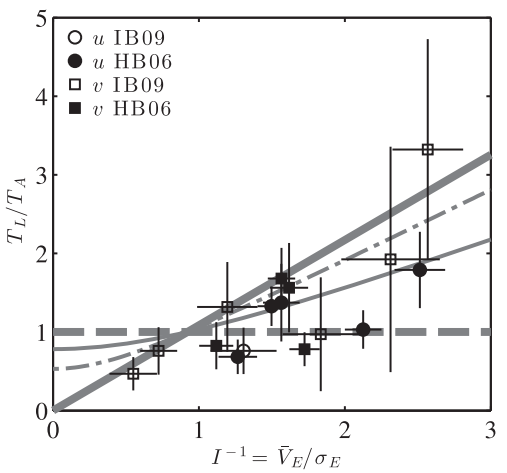

Figure 9. The Lagrangian to apparent-Eulerian time scale ratio (T_L/T_A) versus the inverse turbulence intensity ($I^{-1} = \bar{V}_E/\sigma_E$). For the cross-shore time scale ratio (circles), the abscissa is $\bar{V}_E/\sigma_{Eu}$ and for the alongshore ratio (squares) it is $\bar{V}_E/\sigma_{Ev}$. Crosshairs are the estimated sampling error. The squared correlation between T_L/T_A and I^{-1} is 0.54 for all the data. Middleton's formula (15) for $\alpha = 0$ (thick dashed), $\alpha = 0.5$ (solid), $\alpha = 1$ (dash-dotted), and $\alpha \to \infty$ (thick solid) are shown.

Moreover, differences from Middleton's relationship between T_L/T_A and I^{-1} (developed for unbounded, isotropic, homogeneous, and stationary turbulence) are expected in the surfzone. One, the eddy field considered here is bounded by a shoreline which can lead to non-Gaussian displacements [*Spydell and Feddersen*, 2012]—a potential explanation for the observed HB06 non-Gaussian displacements [*Spydell et al.*, 2009]. Two, the eddy field considered here is neither stationary nor homogeneous (e.g., Figure 4). However, the data presented here are not sufficient (error bars in Figure 9) to discern deviations from Middleton's approximate theory.

5. Discussion

5.1. Comparing Surfzone α

As turbulence is usually described from an Eulerian perspective, e.g., a wave number

spectra, and often sampled with Eulerian instruments, parameterizing eddy diffusivities (a Lagrangian property) in terms of the underlying Eulerian turbulent properties is an important goal for oceanographic research. The parameterization of eddy diffusivities in terms of Eulerian statistics depends on the parameter $\alpha = \sigma T_E / L_E$. Hence, α is a fundamental quantity in surfzone two-dimensional dispersion. For these observations based on a cross-shore array of current meters, α cannot be determined directly from Eulerian statistics because: (1) estimating the alongshore Eulerian length scale $L_E^{(y)}$ is not possible and (2) for $V \neq 0$, current meters measure T_A rather than T_E. To estimate alongshore T_E and L_E requires an alongshore array of current meters. To accurately resolve the eddy length scale, a 200 m long array with instrument spacing <30 m would be required as L_E may be as small as 30 m. Such an array has been deployed at Duck, NC [e.g., *Noyes et al*., 2004; *MacMahan et al*., 2010] but Lagrangian data were not collected. Surfzone T_E and L_E could also be estimated from numerical model simulations. Although α cannot be directly determined from the HB06 and IB09 observations, from the HB06 and IB09 values of T_L/T_A and $I^{-1} = \bar{V}/\sigma_E$, the α inferred from (15) suggests the entire range $(0 - \infty)$ of α (gray curves in Figure 9). However, errors in T_L/T_A and I^{-1} can overlap the entire α range (vertical and horizontal error bars in Figure 9, respectively), leading to uncertainty regarding variation in α. Moreover, Middleton's expressions for relating T_L to Eulerian quantities (11 and 15) are for idealized isotropic covariances resulting in $q = (\pi/8)^{1/2}$ which may not be applicable in the surfzone. Also, other methodologies yield different time scale estimates. For example, relative to the time scales based on a Lagrangian stochastic model [*Spydell and Feddersen*, 2012], the time scales here are on average 41% lower in the cross-shore and 27% higher in the alongshore. Stochastic model time scale estimates are based on minimizing the difference between modeled and observed diffusivities whereas here a simple exponential is fit to the observed autocovariance. Although different in magnitude, due to calculation method, both daily cross-shore and daily alongshore stochastic model time scales and the time scales calculated here are correlated indicating that both are measures of how quickly surfzone Lagrangian velocities decorrelate. The analysis here cannot constrain a surfzone α to be in either fixed-float or frozen-field. However, *Clark et al*. [2010] found that the surfzone dye-tracer cross-shore diffusivity K_x correlated moderately ($r^2 = 0.6$) with a mixing-length scaling $K_x = 0.2\sigma L_{sz}$ (with a surfzone width of $L_{sz} \approx 100$ m), suggesting that the surfzone is frozen field. Unfortunately, the data analyzed here, and in *Clark et al*. [2010], is insufficient to determine with confidence whether the surfzone is fixed float or frozen field.

Other oceanographic regions span a similarly large range of α. From N. Atlantic Eulerian satellite-based surface observations, *Lumpkin et al*. [2002] found fixed-float ($\alpha < 0.5$) values for 10% of the observations, frozen-field values ($1 < \alpha < 2$) in energetic eddy regions like the Gulf stream extension, and intermediate α (0.5–1.0) elsewhere. However, *Chiswell et al*. [2007] suggests that Lumpkin's α values may be biased low due to T_E estimation method [*Stammer*, 1997]. Data consistent with frozen-field turbulence ($\alpha > 1$) has also been found for observations off California [*Davis*, 1985], near New Zealand [*Chiswell et al*., 2007], and near the Antarctic Circumpolar Current [*Sallée et al*., 2008]. Thus, variation in α is common, with larger α ("frozen-field" values) associated with increased eddy activity.

5.2. Modeling Surfzone Tracer Dispersion and Dilution

A long-term practical goal is to model, without extensive numerical simulations, the transport and dilution of surfzone tracers given wave conditions and bathymetry. This has particular relevance for the evolution of surfzone fecal indicator bacteria concentration [e.g., *Grant et al*., 2005; *Rippy et al*., 2013a] or for beach macrofauna larval connectivity in nearshore regions [*Defeo and McLachlan*, 2005], analogous to fish larval connectivity in coastal waters [*Watson et al*., 2010]. Simplified models would allow rapid, qualitative analysis of surfzone tracer dispersion and exchange for a range of wave and tide conditions. Recent work has shown that observed surfzone dispersion is well represented by an advection diffusion equation [*Clark et al*., 2010] and by a Lagrangian stochastic model [*Spydell and Feddersen*, 2012]. In these models, tracer or particles are advected by the mean alongshore current V and spread in both horizontal directions by an eddy diffusivity K. Thus, for given $V(x)$, K, and a specified tracer source, surfzone tracer concentrations are readily solved for.

If the incident wave field and bathymetry are known, wave driven $V(x)$ can be well modeled on planar and barred alongshore homogeneous beaches [e.g., *Thornton and Guza*, 1986; *Ruessink et al*., 2001]. To determine the turbulent eddy diffusivity $K = \sigma^2 T_L$, both the eddy velocity and the Lagrangian time scale are required. Although $\sigma_L = \sigma_E$ can be assumed, the dependence of σ on incident wave conditions is not well understood. However, recent research has indicated that for weak alongshore currents, σ_E is

related to the offshore significant wave height [*MacMahan et al*., 2010] and period [*de Schipper et al*., 2012]. For stronger V, surfzone σ_E is related to V [*Noyes et al*., 2004]. These initial results suggest it is possible to parameterize σ in terms of incident waves. In order to parameterize the eddy diffusivity K, the Lagrangian time scale must also be specified. However, it is not known how surfzone T_L (and therefore K) should be parameterized. Observations constrain T_L to 100–400 s (Figures 8a and 8b), with cross-shore values at the lower end of the range. Although, the work here suggests that it may be possible to parameterize T_L from surfzone Eulerian eddy statistics, i.e., σ, T_E, and L_E, it is unknown how T_L depends on the incident wave field nor is known how T_E and L_E depend on the incident waves. In order to better parameterize surfzone K in terms of the incident wave field, future work aims to explore the relationship between incident waves and both Lagrangian (T_L) and Eulerian eddy statistics (T_E and L_E).

6. Summary

Concurrent Lagrangian and Eulerian observations of rotational, low-frequency ($<$0.01 Hz) surfzone eddies are compared. Surface drifters were tracked for a few hours on each of 11 days at two alongshore uniform beaches. A cross-shore array of near-bottom current meters extended from near the shoreline to seaward of the surfzone. Lagrangian and Eulerian cross-shore dependent mean alongshore velocities $V(x)$ are similar as well as bulk daily mean alongshore velocities $\bar{V}$. Cross-shore dependent Lagrangian $s_{Lu}(x)$ and Eulerian $s_{Eu}(x)$ eddy velocities, estimated from low-pass filtered drifter and current meter velocities, respectively, are similar (Figures 5c and 5d). Cross-shore rotational velocities have a midsurfzone maximum whereas alongshore rotational velocities are distributed more broadly. Daily Lagrangian and apparent-Eulerian cross-shore and alongshore time scales T were found by fitting the bulk low-frequency velocity autocovariance functions to an exponential. Daily estimates of the Lagrangian time scale vary between 50 and 300 s depending on the day and direction (cross-shore or alongshore). The ratio of Lagrangian to apparent Eulerian current meter decorrelation times T_L/T_A varies considerably, between about 0.5 and 3 and some of the variation is ascribable to the relatively large range of V/σ of these observations. With large V, T_A is a measure of the time for an eddy to advect past a current meter and is less than the time a drifter spends in an eddy T_L, thus $T_L/T_A > 1$. With small V/σ, the situation is reversed and $T_L/T_A < 1$. Alongshore advection effects are detectable in the present T_L/T_A observations, but estimates of T_L/T_A vary between days with similar V/σ suggesting that surfzone Lagrangian particle dynamics vary between days, spanning the range from "fixed-float" to "frozen-field" [*Middleton*, 1985]. Given values of T_L/T_A and $I^{-1} = \bar{V}/\sigma_E$, α can be inferred from (15), however, statistical errors in both T_L/T_A and I^{-1} (error bars in Figure 9) lead to uncertainty regarding variation in α. Furthermore, Middleton's expressions (11 and 15) relating T_L to Eulerian quantities are for idealized isotropic covariances and may not be completely applicable in the surfzone.

The results here indicate that Lagrangian and Eulerian statistics, in particular time scales, are related in the surfzone (the data in Figure 9 can be fit with a single curve). Thus, parameterizing the surfzone eddy diffusivity with Eulerian statistics is likely possible but the observations here are not sufficient to discern the precise relationship (e.g., α). Moreover, the exact relationship between surfzone Eulerian and Lagrangian statistics is unknown and a complete description requires understanding how the dependence of the Eulerian eddy time scale T_E and length scale L_E depend on the incident wave field. Drifter measurements within cross-shore and alongshore current meter arrays are required to observationally relate surfzone diffusivity to T_E and L_E. Suitable current meter arrays have been deployed [e.g., *Noyes et al*., 2004; *MacMahan et al*., 2010], but concurrent drifter observations are not available. Although a complete analysis relating Eulerian and Lagrangian statistics is not possible from existing observations, numerical simulations with a wave-resolving model that accurately represent surfzone Eulerian and Lagrangian statistics [*Spydell and Feddersen*, 2009; *Feddersen et al*., 2011; *Clark et al*., 2011; *Feddersen*, 2013] can be used to estimate all of the relevant statistics (e.g., σ, T_E, L_E, and T_L) required to relate Eulerian and Lagrangian eddy properties.

Appendix A: Sampling Errors

Sampling errors for Eulerian and Lagrangian statistics are calculated by Monte Carlo simulation. Ensembles of Eulerian and Lagrangian velocity time series are generated assuming that velocities follow the stochastic differential equation (Langevin equation)

$$\frac{du}{dt} = -\frac{u}{T} + \sqrt{\frac{2\sigma^2}{T}}w \tag{A1}$$

where u is the Eulerian or Lagrangian velocity, either cross-shore or alongshore, T is the time scale, σ^2 is the velocity variance, and w is a zero mean, stationary, white noise process with unit variance. The autocovariance function $C(t)$ of the stochastic process (A1) is $C(t)=\sigma^2\exp(-t/T)$, which is used to fit the observed $C(t)$ (19).

For each day of drifter observations, a daily data set of simulated $u_L(t)$ and $v_L(t)$ are generated with (A1) using the observed σ_L^2 and T_L (Figures 7 and 8). The bulk daily value of $\bar{V}_L$ (Figure 6) is added to each simulated $v(t)$. The number and length of simulated Lagrangian velocity time series matches the observations. For each daily simulated Lagrangian velocity data set, a realization of the mean velocity $\hat{V}_L$ and cross-shore and alongshore autocovariance functions $\hat{C}_L(t)$ are calculated exactly as done for the observations. From $\hat{C}_L(t)$, simulated $\hat{T}_L$ and $\hat{\sigma}_L^2$ are found by best fitting, hence, $\hat{V}_L, \hat{C}_L(t), \hat{\sigma}_L^2$, and $\hat{T}_L$ are each a single realization of the mean Lagrangian velocity, daily autocovariance function, velocity variance, and time scale, respectively. This process is repeated 1000 times yielding an ensemble of these quantities. The average (or expectation) over repeated experiments is denoted by $E[]$, and for V_L and $C(t)$ it is unbiased, i.e., $E[\hat{V}_L]=\bar{V}_L$ and $E[\hat{C}(t)]=\sigma_L^2\exp(-t/T_L)$, where $\bar{V}_L, \sigma_L^2$, and T_L are the values initially prescribed. The sampling error ϵ is defined by standard deviation, i.e., for the bulk mean alongshore velocity $\epsilon_{\bar{V}_L}=\mathrm{std}[\hat{V}_L]=\{E[(\hat{V}_L-\bar{V}_L)^2]\}^{1/2}$. Sampling errors of the Lagrangian autocovariance function are shown in Figure 3 (thin solid lines are $C_L(t)\pm\epsilon_{C_L}(t)$), of the mean alongshore velocity in Figure 6 (thin vertical lines are $\bar{V}_L\pm\epsilon_{\bar{V}_L}$), and of the velocity variance and time scale in Figures 7 and 8 (vertical lines), respectively. The Lagrangian sampling errors are biased small as not all drifters were sufficiently separated to be considered independent, which this analysis assumes. Thus, the Lagrangian sampling errors presented here are lower bounds on the true sampling error.

Sampling errors for Eulerian quantities are found in a similar manner by generating simulated time series of $u_{E,ij}(t)$ and $v_{E,ij}(t)$ for each instrument i and hour j using the daily σ_E^2 and T_A in (A1). The bulk daily mean Eulerian alongshore velocity $\bar{V}_E$ is then added to each $v_{E,ij}(t)$. Time averaging each $v_{E,ij}(t)$ then yields $\hat{V}_{E,ij}$ from which a realization of $\hat{V}_E$ is found using (21). From a simulated daily Eulerian velocity data set, a realization of $\hat{V}_E, \hat{C}_E(t), \hat{\sigma}_E^2$, and $\hat{T}_A$ is determined in the same manner as for the Eulerian observations. Repeating this yields an ensemble of these quantities, the standard deviation of which is the sampling error of the Eulerian quantities and shown in Figures 6–8.

Sampling errors for T_L/T_A and I^{-1} are calculated by determining $\hat{T}_L/\hat{T}_A$ and $\hat{I}_u^{-1}=\hat{V}/\hat{\sigma}_E$ for each member of the ensemble and then taking the standard deviation. Sampling errors for T_L/T_A and I^{-1} are indicated by thin vertical and horizontal lines in Figure 9, respectively.

Acknowledgments

This analysis was supported by NSF, ONR, and CA Sea Grant. The HB06 field work was supported by CA Coastal Conservancy, NOAA, NSF, ONR, and CA Sea Grant. R. T. Guza was a co-PI on the HB06 experiment. Staff and students from the Integrative Oceanography Division (B. Woodward, B. Boyd, K. Smith, D. Darnell, I. Nagy, D. Clark, M. Omand, M. Yates, M. McKenna, M. Rippy, and S. Henderson) and the Naval Postgraduate School (J. Brown and B. Swick) were instrumental in acquiring the field observations. The comments from three reviewers improved this manuscript and are greatly appreciated.

References

Abernathey, R. P., and J. Marshall (2013), Global surface eddy diffusivities derived from satellite altimetry, *J. Geophys. Res.*, *118*, 901–916, doi:10.1002/jgrc.20066.

Anfossi, D., U. Rizza, C. Mangia, G. A. Degrazia, and E. Pereira Marques Filho (2006), Estimation of the ratio between the Lagrangian and Eulerian time scales in an atmospheric boundary layer generated by large eddy simulation, *Atmos. Environ.*, *40*(2), 326–337, doi:10.1016/j.atmosenv.2005.09.041.

Brown, J., J. MacMahan, A. Reniers, and E. Thornton (2009), Surf zone diffusivity on a rip-channeled beach, *J. Geophys. Res.*, *114*, C11015, doi:10.1029/2008JC005158.

Chiswell, S. M., and G. J. Rickard (2008), Eulerian and Lagrangian statistics in the Bluelink numerical model and AVISO altimetry: Validation of model eddy kinetics, *J. Geophys. Res.*, *113*, C10024, doi:10.1029/2007JC004673.

Chiswell, S. M., G. J. Rickard, and M. M. Bowen (2007), Eulerian and Lagrangian eddy statistics of the Tasman Sea and southwest Pacific Ocean, *J. Geophys. Res.*, *112*, C10004, doi:10.1029/2007JC004110.

Clark, D. B., F. Feddersen, and R. T. Guza (2010), Cross-shore surfzone tracer dispersion in an alongshore current, *J. Geophys. Res.*, *115*, C10035, doi:10.1029/2009JC005683.

Clark, D. B., F. Feddersen, and R. T. Guza (2011), Modeling surfzone tracer plumes, part 2: Transport and dispersion, *J. Geophys. Res.*, *116*, C11028, doi:10.1029/2011JC007211.

Corrsin, S. (1959), Progress report on some turbulent diffusion research, in *Advances in Geophysics*, vol. *6*, edited by H. E. Landsberg, pp. 161–162, Academic, New York.

Davis, R. E. (1982), On relating Eulerian and Lagrangian velocity statistics: Single particles in homogeneous flows, *J. Fluid Mech.*, *114*, 1–26, doi:10.1017/S0022112082000019.

Davis, R. E. (1983), Oceanic property transport, Lagrangian particle statistics, and their prediction, *J. Mar. Res.*, *41*(C11), 163–194.

Davis, R. E. (1985), Drifter observations of coastal surface currents during CODE: The statistical and dynamical views, *J. Geophys. Res.*, *90*, 4756–4772.

de Schipper, M., A. Reniers, J. MacMahan, and R. Ranasinghe (2012), Vortical VLF motions under shore-normal incident waves, in *Proceedings of the 33rd Conference on Coastal Engineering, ICEE*, edited by P. Lynett and J. McKee Smith, pp. 1–13, Coast. Eng. Res. Counc., Reston, Va.

Defeo, O., and A. McLachlan (2005), Patterns, processes and regulatory mechanisms in sandy beach macrofauna: A multi-scale analysis, *Mar. Ecol. Prog. Ser.*, *295*, 1–20, doi:10.3354/meps295001.

Dever, E. P., M. C. Hendershott, and C. D. Winant (1998), Statistical aspects of surface drifter observations of circulation in the Santa Barbara channel, *J. Geophys. Res.*, *103*(C11), 24,781–24,797, doi:10.1029/98JC02403.

Feddersen, F. (2012a), Scaling surfzone dissipation, *Geophys. Res. Lett.*, *39*, L18613, doi:10.1029/2012GL052970.

Feddersen, F. (2012b), Observations of the surfzone turbulent dissipation rate, *J. Phys. Oceanogr.*, *42*, 386–399, doi:10.1175/JPO-D-11–082.1.

Feddersen, F. (2013), The generation of surfzone eddies in a strong alongshore current, *J. Phys. Oceanogr.*, *44*(2), 600–617, doi:10.1175/JPO-D-13-051.1.

Feddersen, F., D. B. Clark, and R. T. Guza (2011), Modeling surf zone tracer plumes: 1. Waves, mean currents, and low-frequency eddies, *J. Geophys. Res.*, *116*, C11027, doi:10.1029/2011JC007210.

Feng, Z., A. Reniers, B. K. Haus, and H. Solo-Gabriele (2013), Modeling sediment-related enterococci loading, transport and inactivation at an embayed non-point source beach, *Water Resour. Res.*, *49*, 693–712, doi:10.1029/2012WR012432.

Ferrari, R., and M. Nikurashin (2010), Suppression of eddy diffusivity across jets in the Southern Ocean, *J. Phys. Oceanogr.*, *40*(7), 1501–1519, doi:10.1175/2010JPO4278.1.

Garraffo, Z. D., A. J. Mariano, A. Griffa, C. Veneziani, and E. P. Chassignet (2001), Lagrangian data in a high-resolution numerical simulation of the North Atlantic, I. Comparison with in situ drifter data, *J. Mar. Syst.*, *29*, 157–176, doi:10.1016/S0924-7963(01)00015-X.

Grant, S. B., J. H. Kim, B. H. Jones, S. A. Jenkins, J. Wasyl, and C. Cudaback (2005), Surf zone entrainment, along-shore transport, and human health implications of pollution from tidal outlets, *J. Geophys. Res.*, *110*, C10025, doi:10.1029/2004JC002401.

Koeltzsch, K. (1998), On the relationship between the Lagrangian and Eulerian time scale, *Atmos. Environ.*, *33*(1), 117–128, doi:10.1016/S1352–2310(98)00135-6.

Ledwell, J. R., E. T. Montgomery, K. L. Polzin, L. C. St. Laurent, R. W. Schmitt, and J. M. Toole (2000), Evidence for enhanced mixing over rough topography in the abyssal ocean, *Nature*, *403*, 179–182, doi:10.1038/35003164.

Lippmann, T. C., T. H. C. Herbers, and E. B. Thornton (2009), Gravity and shear wave contributions to nearshore infragravity motions, *J. Phys. Oceanogr.*, *29*(2), 231–239.

Lumpkin, R., A. Treguier, and K. Speer (2002), Lagrangian eddy scales in the northern Atlantic Ocean, *J. Phys. Oceanogr.*, *32*(9), 2425–2440.

Lundgren, T. S., and Y. B. Pointin (1976), Turbulent self-diffusion, *Phys. Fluids*, *19*, 355–358.

Ma, G., F. Shi, and J. Kirby (2011), A polydisperse two-fluid model for surf zone bubble simulation, *J. Geophys. Res.*, *116*, C05010, doi:10.1029/2010JC006667.

MacMahan, J., J. Brown, and E. B. Thornton (2009), Low-cost handheld global positioning systems for measuring surf zone currents, *J. Coastal Res.*, *25*, 744–754, doi:10.2112/08-1000.1.

MacMahan, J. H., A. J. H. M. Reniers, and E. B. Thornton (2010), Vortical surf zone velocity fluctuations with 0(10) min period, *J. Geophys. Res.*, *115*, C06007, doi:10.1029/2009JC005383.

Marshall, J., E. Shuckbergh, H. Jones, and C. Hill (2006), Estimates and implications of surface eddy diffusivity in the southern ocean derived from tracer transport, *J. Phys. Oceanogr.*, *36*, 1806–1821, doi:10.1175/JPO2949.1.

Middleton, J. F. (1985), Drifter spectra and diffusivities, *J. Mar. Res.*, *43*(1), 37–55.

Noyes, T. J., R. T. Guza, S. Elgar, and T. H. C. Herbers (2004), Field observations of shear waves in the surf zone, *J. Geophys. Res.*, *109*, C01031, doi:10.1029/2002JC001761.

Noyes, T. J., R. T. Guza, F. Feddersen, S. Elgar, and T. H. C. Herbers (2005), Model-data comparisons of shear waves in the nearshore, *J. Geophys. Res.*, *110*, C05019, doi:10.1029/2004JC002541.

Omand, M. M., J. J. Leichter, P. J. S. Franks, A. J. Lucas, R. T. Guza, and F. Feddersen (2011), Physical and biological processes underlying the sudden appearance of a red-tide surface patch in the nearshore, *Limnol. Oceanogr.*, *56*, 787–801.

Philip, J. R. (1967), Relation between Eulerian and Lagrangian statistics, *Phys. Fluids*, *10*, S69–S71.

Pope, S. (1994), Lagrangian PDF methods for turbulent flows, *Annu. Rev. Fluid Mech.*, *26*(1), 23–63.

Rippy, M. A., P. J. S. Franks, F. Feddersen, R. T. Guza, and D. F. Moore (2013a), Factors controlling variability in nearshore fecal pollution: Fecal indicator bacteria as passive particles, *Mar. Pollut. Bull.*, *66*, 151–157, doi:10.1016/j.marpolbul.2012.09.030.

Rippy, M. A., P. J. S. Franks, F. Feddersen, R. T. Guza, and J. A. Warrick (2013b), Beach nourishment impacts on bacteriological water quality and phytoplankton bloom dynamics, *Environ. Sci. Technol.*, *47*, 6146–6154, doi:10.1021/es400572k.

Ruessink, B. G., J. R. Miles, F. Feddersen, R. T. Guza, and S. Elgar, Modeling the alongshore current on barred beaches, *J. Geophys. Res.*, *106*, 22,451–22,463.

Rypina, I. I., I. Kamenkovich, P. Berloff, and L. J. Pratt (2012), Eddy-induced particle dispersion in the near-surface North Atlantic, *J. Phys. Oceanogr.*, *42*(12), 2206–2228, doi:10.1175/JPO-D-11-0191.1.

Saffman, P. G. (1963), An approximate calculation of the Lagrangian auto-correlation coefficient for stationary, homogeneous turbulence, *Appl. Sci. Res.*, *A11*, 245–255.

Sallée, J. B., K. Speer, R. Morrow, and R. Lumpkin (2008), An estimate of Lagrangian eddy statistics and diffusion in the mixed layer of the Southern Ocean, *J. Mar. Res.*, *66*(4), 441–463.

Schmidt, W. E., B. T. Woodward, K. S. Millikan, R. T. Guza, B. Raubenheimer, and S. Elgar (2003), A GPS-tracked surf zone drifter, *J. Atmos. Oceanic Technol.*, *20*(7), 1069–1075.

Spydell, M., and F. Feddersen (2009), Lagrangian drifter dispersion in the surf zone: Directionally spread, normally incident waves, *J. Phys. Oceanogr.*, *39*, 809–830.

Spydell, M. S., and F. Feddersen (2012), A Lagrangian stochastic model of surf zone drifter dispersion, *J. Geophys. Res.*, *117*, C03041, doi:10.1029/2011JC007701.

Spydell, M. S., F. Feddersen, R. T. Guza, and W. E. Schmidt (2007), Observing surf-zone dispersion with drifters, *J. Phys. Oceanogr.*, *37*, 2920–2939.

Spydell, M. S., F. Feddersen, and R. T. Guza (2009), Observations of drifter dispersion in the surfzone: The effect of sheared alongshore currents, *J. Geophys. Res.*, *114*, C07028, doi:10.1029/2009JC005328.

Stammer, D. (1997), Global characteristics of ocean variability estimated from regional TOPEX/POSEIDON Altimeter measurements, *J. Phys. Oceanogr.*, *27*(8), 1743–1769.

Taylor, G. I. (1922), Diffusion by continuous movements, *Proc. London Math. Soc.*, *20*, 196–212.

Thornton, E. B., and R. T. Guza (1986), Surf zone longshore currents and random waves: Field data and models, *J. Phys. Oceanogr.*, *16*(7), 1165–1178.

Watson, J. R., S. Mitarai, D. A. Siegel, J. E. Caselle, C. Dong, and J. C. McWilliams, Realized and potential larval connectivity in the Southern California Bight, *Mar. Ecol. Prog. Ser.*, *401*, 31–48, doi:10.3354/meps08376.

Weinstock, J. (1976), Lagrangian-Eulerian relations and the independence approximation, *Phys. Fluids*, *19*, 1702–1711.

Wunch, C., and R. Ferrari (2004), Vertical mixing, energy, and the general circulation of the ocean, *Annu. Rev. Fluid Mech.*, *36*, 281–314, doi: 10.1146/annurev.fluid.36.050802.122121.

Zhang, Q. (1995), Transient behavior of mixing induced by a random velocity field, *Water Resour. Res.*, *31*, 557–591, doi:10.1029/94WR02275.

Zhurbas, V., and I. S. Oh (2004), Drifter-derived maps of lateral diffusivity in the Pacific and Atlantic Oceans in relation to surface circulation patterns, *J. Geophys. Res.*, *109*, C05015, doi:10.1029/2003JC002241.